

# Study of water adsorption and capillary bridge formation for SiO<sub>2</sub> nanoparticle layers by means of a combined *in situ* FT-IR reflection spectroscopy and QCM-D set-up†

Cite this: *Phys. Chem. Chem. Phys.*,  
2014, 16, 7377

B. Torun,<sup>a</sup> C. Kunze,<sup>a</sup> C. Zhang,<sup>b</sup> T. D. Kühne<sup>b</sup> and G. Grundmeier<sup>\*a</sup>

Water adsorption and capillary bridge formation within a layer of SiO<sub>2</sub>-nanoparticles were studied *in situ* by means of a combination of quartz crystal microbalance (QCM-D) with dissipation analysis and Fourier transformation infrared reflection absorption spectroscopy (FT-IRRAS). FT-IR data were employed to distinguish the “ice-like” and “liquid-like” contributions and to support the analysis of the QCM-D data concerning mass change and dissipation. Combined measurements show that for SiO<sub>2</sub>-nanoparticles with a diameter of about 250 nm, the formation of two adsorbed monolayers of water as well as bulk water leads to a rather linear increase in the dissipation for relative humidity values of up to 60% which is followed by a strong increase in dissipation during the actual liquid bridge formation. Subsequently, the dissipation drops again when the relative humidity is further increased to values >90%.

Received 20th November 2013,  
Accepted 24th February 2014

DOI: 10.1039/c3cp54912g

www.rsc.org/pccp

## Introduction

During the past decade nanoparticles have attracted much attention and found many industrial applications in various fields ranging from pigments and antibacterial agents in clothes<sup>1,2</sup> to highly efficient catalysts.<sup>3,4</sup> In general, the special characteristics of these small particles derive from their high surface to volume ratio in contrast to macroscopic particles. In the context of handling and processing such nanoparticle powders the flow properties play an important role.

Flow characteristics of microparticle ensembles are strongly dependent on the particle–particle interaction forces. These forces strongly vary not only with the particle material properties but also with its surface chemical composition as well as with the environmental conditions.

The theory of the fundamental interacting forces, which in most cases are based on electrostatic and van der Waals forces, and their force–distance relationships have been reviewed in great detail by Israelachvili in his monograph on “Intermolecular and Surface Forces”.<sup>5</sup> The measurement of interaction forces between individual microscopic particles mainly based

on AFM methods attracted much attention in the last few years and was reviewed by Butt and Kappel.<sup>6,7</sup>

In the literature, quartz crystal microbalance (QCM) studies addressing both the study of particle adsorption as well as investigation of collective particle behavior are discussed. For the latter, QCM was utilized by Johannsmann *et al.*<sup>8,9</sup> where they found a hysteretic increase in contact strength between particles and a quartz crystal during cycles of varying relative humidity. This behavior was explained by contact stiffening due to capillary forces inducing an increase in the effective contact area between the particle and the substrate with every cycle. Moreover, the same group<sup>9</sup> could follow the transition from elastic to inertial loading as predicted by the Dybwad model.<sup>10</sup> During their experiment, they wetted a layer of 100 μm sized spheres on a torsional resonator and measured the frequency shift ( $\Delta f$ ) and the dissipation ( $D$ ) while the sample was slowly drying. It was found that the dissipation, which is directly correlated with the half-band-half-width  $\Gamma$  and the resonance frequency  $f_r$  (eqn (1)), exhibits a local maximum during the drying process.

$$D = \frac{2\Gamma}{f_r} \quad (1)$$

They attributed this maximum to the transition from the Dybwad state (weak contact) to the Sauerbrey state (strong contact). Moreover, they explained the change in contact force to be a result of the drying process inducing the formation of capillaries. As a result, the force between the particles and the substrate increases continuously as the sample dries resulting in the transition from elastic to inertial loading.

<sup>a</sup> Technical and Macromolecular Chemistry, University of Paderborn, Warburger Str. 100, 33098 Paderborn, Germany.

E-mail: guido.grundmeier@tc.uni-paderborn.de

<sup>b</sup> Institute of Physical Chemistry and Center for Computational Sciences, Johannes Gutenberg University Mainz, Staudinger Weg 7, 55128 Mainz, Germany

† Electronic supplementary information (ESI) available. See DOI: 10.1039/c3cp54912g



Focusing on the particle adsorption onto quartz crystal surfaces, Pomorska *et al.*<sup>11</sup> studied the adsorption of mesoporous TiO<sub>2</sub> nanocontainers modified with polyelectrolyte layers on self-assembled monolayer modified quartz crystals. They found an interesting effect resulting in a positive frequency shift of the resonator during the adsorption of micrometer sized objects from solution.<sup>12</sup> This effect was attributed to a resonance between the adsorbed colloids and the resonator. It was concluded that for large objects (>1 µm) the observed frequency shift depends on the contact stiffness instead of the absolute mass change.

The valuable information regarding the QCM with dissipation analysis (QCM-D) however mostly lacks the simultaneous *in situ* spectroscopic analysis of the particle films. FT-IR-spectroscopy in reflection mode is a well-established tool for the analysis of water adsorption on various surfaces. Asay *et al.*<sup>13</sup> investigated the evolution of the water layer structure on silicon oxide. They found that at lower relative humidity the water structure was dominated by the so called “ice-like” structure whereas for higher relative humidity the “liquid-like” water structure was preferred. In another study reported by Giner *et al.*<sup>14</sup> the influence of a plasma modification of aluminum surfaces on the water adsorption was investigated by means of *in situ* PM-IRRAS combined with QCM. It was found that the amount of adsorbed water varies with the degree of surface hydroxylation. Moreover, the diffusion of water through protecting surface coatings and barrier film properties of these layers are of crucial interest in the case of corrosion protection for engineering materials.<sup>15,16</sup> Liu *et al.*<sup>17</sup> studied the barrier properties of ultra-thin SiO<sub>x</sub> plasma polymer layers towards water penetration using DPM-FT-IRRAS to characterize the water uptake. In addition to the studies on water adsorption and barrier penetration, more fundamental studies have focused on the structure of water and the properties of the formed hydrogen bond-network mostly by means of FT-IR and Raman spectroscopy techniques.<sup>18,19</sup> In their comprehensive work, Chumaevskii *et al.*<sup>18</sup> investigated the shape of the Raman peak of liquid water with different salts and deconvoluted it with respect to the different conformers of water in the network. Moreover, they argue that the two bonds of the water molecule are not equal and behave as independent oscillators.

The presented study focusses on the correlation between the FT-IR-data of the water adsorbate layer and the QCM-D data. SiO<sub>2</sub>-nanoparticle films were chosen as a reference system due to their reproducible surface chemistry and monodispersity.

## Experimental

### Materials and chemicals

Chemicals were of analytical grade and used without further purification. Ultrapure water with a typical conductivity of 0.055 µS cm<sup>-1</sup> was obtained from a water purification system (Ultraclear TWF, SG Wasseraufbereitung, Barsbüttel, Germany). Water based dispersions (50 mg ml<sup>-1</sup>) of monodisperse SiO<sub>2</sub> particles with a diameter of 250 nm were purchased from microParticles GmbH (Berlin, Germany). 5 MHz 1 inch AT-cut

QCM-crystals with a Cr/Au coating were obtained from Fil-Tech Inc. (Boston, USA). Chemical compounds used like Hexamethyldisiloxane (HMDSO) and octadecanethiol (ODT) have been supplied by Sigma Aldrich (St. Louis, USA).

### Sample preparation

In order to remove organic contaminations, QCM-crystals were cleaned by means of a mixture of 1:1 of 30% aqueous NH<sub>3</sub> and 30% aqueous H<sub>2</sub>O<sub>2</sub> (Caution: this mixture is extremely corrosive). The solution was heated to 70 °C and crystals were immersed for approximately 1 to 2 hours before use followed by extensive rinsing with ultrapure water, ethanol and blow-drying in a stream of nitrogen. Subsequently, crystals were coated *via* plasma enhanced chemical vapor deposition (PE-CVD) with a thin layer of a SiO<sub>2</sub> plasma polymer using hexamethyldisiloxane (HMDSO) as a precursor. Deposition was performed using a gas composition with a high O<sub>2</sub> excess with respect to the precursor to ensure the formation of an inorganic glass-like film. Initially, Ar was supplied to the plasma cell at a flow rate of 0.9 ml min<sup>-1</sup> and the pumping rate was adjusted to establish a stable pressure of 0.15 mbar. Then O<sub>2</sub> was dosed until the total pressure reached 0.3 mbar. Finally, HMDSO was dosed increasing the pressure for additional 0.005 mbar and the plasma (500 V, 4 mA, 4 kHz) was ignited for 10 minutes. Surface chemistry of the deposited thin SiO<sub>2</sub> layer was analyzed by means of X-ray photoelectron spectroscopy (XPS) and infrared spectroscopy (FT-IR). Moreover, morphology was characterized by field emission scanning electron microscopy (FE-SEM) and atomic force microscopy (AFM). A reference sample for FT-IR experiments was prepared by means of solution self-assembly of 1-octadecanethiol (ODT) on the gold coated bare QCM-crystal (Fig. 1). Cleaned crystals were immersed in 1 mmol ethanolic solution of ODT. After 24 hours, crystals were removed from solution and rinsed with pure ethanol before drying in a gentle stream of nitrogen. ODT surfaces typically yielded a static water contact angle of about 110 degrees indicating a highly ordered aliphatic terminated crystalline self-assembled monolayer.

### Particle layer preparation

100 µl of the as received SiO<sub>2</sub> nanoparticle suspension was diluted in 50 ml water together with 16.5 µl of 37% hydrochloric acid followed by sonication for 15 minutes. Plasma polymer modified crystals were immersed in the nanoparticle suspension for 24 hours allowing the particles to sediment on the substrate. Crystals were then carefully removed from the solution and dipped into ultrapure water with an adjusted pH of 2 in order to remove excess particles. Finally, the sample was dried in a gentle stream of nitrogen. This procedure typically yielded a sample with 0.8 to 2 monolayers of particles, mostly in a hexagonal close packing as indicated by FE-SEM. The samples were also checked for contaminations by means of XPS.

### *In situ* combined FT-IR reflection absorption – QCM-D measurements

A new experimental setup (Fig. 2) was designed allowing simultaneous FT-IR reflection and QCM-D measurements of



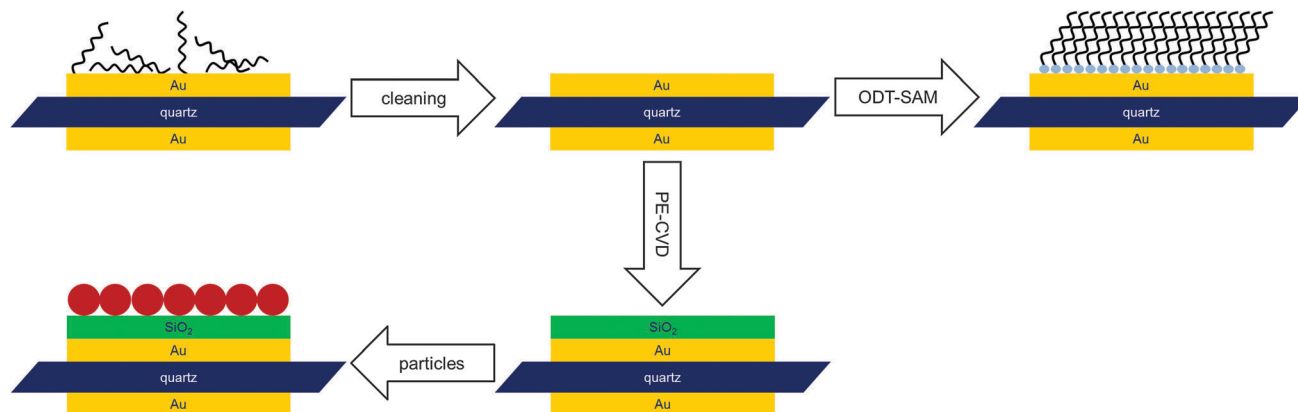


Fig. 1 Schematic of the sample preparation procedure. After cleaning, the samples were coated with a thin SiO<sub>2</sub> film by means of PE-CVD. Water uptake was then analyzed by combined *in situ* QCM-D/FT-IR. Subsequently, the identical sample was modified with SiO<sub>2</sub> particles and water uptake studies were repeated. The ODT covered sample was prepared by solution self-assembly and used as reference for FT-IR-data evaluation.

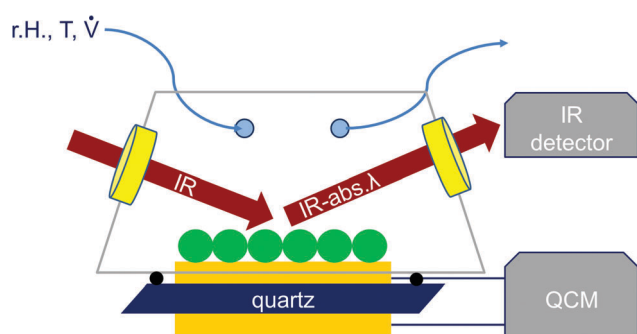


Fig. 2 Schematic of the cell for combined QCM-D/FT-IR measurements. The cell is sealed against the specimen with an O-ring. During an experiment the inner cavity is continuously purged with nitrogen of desired relative humidity and flow rate.

immobilized particle mono- and multilayers. The setup features a small sample compartment which allows for controlling the atmosphere in terms of relative humidity and temperature. The humid air is provided by a custom build humid air generator using nitrogen as carrier gas. Desired relative humidity is generated by mixing streams of dry and humid nitrogen. The gas flow rate was controlled using two mass flow controllers automatically maintaining a desired total flow rate. Temperature and relative humidity were continuously monitored directly within the cell. Two IR-transparent ZnSe windows were installed allowing an FT-IR experiment with a 45° angle of incidence. The cell was fitted in a Bruker Vertex V70 FT-IR spectrometer using an MCT detector. The sample compartment containing the measurement-cell was purged with synthetic CO<sub>2</sub> free dry air at all times.

The cell was sealed against the quartz crystal using a Viton O-ring. At the beginning of a typical experiment, the sample was purged with dry nitrogen at a flow rate of 0.5 l min<sup>-1</sup> and a temperature of 25 °C for 180 minutes. After the resonance frequency of the crystal had stabilized, the humidity was increased stepwise. At each step, an FT-IR spectrum was acquired after the frequency shift had stabilized. In order to neutralize the effect of water adsorption on the ZnSe windows, a reference measurement

was performed using an octadecanethiol self-assembled monolayer modified quartz crystal. Due to the high surface hydrophobicity, almost no water adsorbed to the SAM during the experiment as indicated by the QCM-D. Acquired IR-spectra of the ODT-sample were used as a reference for the FT-IR-evaluation of both the SiO<sub>2</sub> plasma polymer and particle coated sample.

#### Ex situ electron spectroscopy and microscopy

X-Ray photoelectron spectroscopy (XPS) was performed in an ESCA<sup>+</sup> spectrometer (Omicron Nanotechnology, Taunusstein, Germany). XPS spectra were measured using a monochromated Al K $\alpha$  X-ray source with an Energy of 1486.7 eV operated at an output power of 300 W. Photoelectrons were detected on a multi-channel plate detector (Omicron Argus) after passing through an hemispherical electron analyzer with a pass energy of 10 eV. All spectra were calibrated with respect to the C 1s peak position at 284.5 eV as an internal reference.

Scanning electron microscopy was performed using an Agilent 8500 field emitter electron microscope at an acceleration voltage of 1 keV. Surface morphology of the plasma deposited SiO<sub>2</sub> layers was studied using an Agilent 5500 Atomic Force microscope (AFM) equipped with a vibration isolation table. Intermittent contact mode measurements were performed using MicroMash (Innovative solutions Bulgaria Ltd, Sofia, Bulgaria) cantilevers type NSC-19 with a typical force constant of 0.63 N m<sup>-1</sup>.

#### Surface determination by the BET method

Particle surface area determination was performed by means of the BET method using an Autosorb-6B (Quantachrome, Odelzhausen, Germany). As received nanoparticle suspension was dried under vacuum conditions. Subsequently, received particle powder was then heated to 120 °C for 12 h under vacuum conditions to remove residual water. Adsorbed nitrogen volume was measured for every  $p/p_0$  with a step size of 0.02 up to a maximum of 0.99. Subsequently, specific surface area was derived from the first five points of the isotherm adsorption branch by the BET-method.



## Results

### AFM, FT-IR, XPS and FE-SEM characterization of the SiO<sub>2</sub> plasma polymer and nanoparticle layers

Plasma polymer films were found to be very smooth indicated by the RMS roughness of 1.70 nm based on the AFM data (Fig. S1A, ESI†). Reference experiments on Mica-template stripped ultra-smooth Au surfaces (Fig. S1B, ESI†) yielded even smoother plasma polymer surfaces (RMS 0.3 nm) indicating that the surface roughness of the PE-CVD SiO<sub>2</sub> layer modified surface is mainly governed by the underlying substrate.

Chemical composition of the SiO<sub>2</sub> plasma polymer was analyzed by means of grazing incidence FT-IR spectroscopy as presented in Fig. S2 (ESI†). It was found that PE-CVD layers deposited were purely of inorganic nature indicated by the absence of the Si-CH<sub>3</sub> peak at 1277 cm<sup>-1</sup>.<sup>20</sup>

XPS measurements were performed to characterize the chemical composition of the plasma polymer and SiO<sub>2</sub> nanoparticles. PE-CVD SiO<sub>2</sub> modified QCM-crystals were directly introduced into the UHV-system after preparation. However, the preparation of nanoparticle samples for XPS analysis involved additional steps. Nanoparticle powder was obtained by drying off the water from the as received suspension under vacuum conditions. The resulting powder was then stamped into an indium foil and the specimen was then transferred into the UHV system for XPS measurements.

XPS data revealed a high chemical purity of both the prepared PE-CVD surface and the nanoparticles (Fig. S3 and S4, ESI†). In the case of the PE-CVD film, the small carbon content indicates that the precursor has been fully oxidized. This is supported by the fact that the O 1s peak has a low full width at half maximum of 1.5 eV. Moreover, the absence of any Au related signals suggests that the substrate is fully covered by the SiO<sub>2</sub> film.

XPS spectra of the SiO<sub>2</sub> particles revealed a high degree of chemical purity with only a very small amount of carbon contamination. In the detailed spectra, the O 1s signal exhibited a shoulder towards higher binding energies attributed to the presence of surface OH functionalities indicating a polar surface. This is in good agreement with static water contact angle measurements in which the droplet immediately spreads on the particle modified surface.

Particle samples were analyzed by means of FE-SEM prior to a QCM-D/FT-IR experiment in order to estimate the coverage of the substrate. Fig. 3 shows a typical crystal surface after particle deposition.

It was found that the surface was mostly covered with only one layer of particles. In comparison to the amount of particles in the first layer only a few particles are located in a second top layer. Most of the particles in the first layer are in a hexagonal closest packing (hcp) with six spheres in direct contact. However there are also domains in which the packing is not perfectly close and the spheres are lacking some of the neighbors. For the evaluation of the QCM-D data, the total coverage of the sample was estimated to be 1.1 monolayers.

### Water adsorption isotherms on SiO<sub>2</sub> nanoparticle coated substrates

Water adsorption studies were performed on both as prepared SiO<sub>2</sub> plasma polymer films and plasma polymer films coated

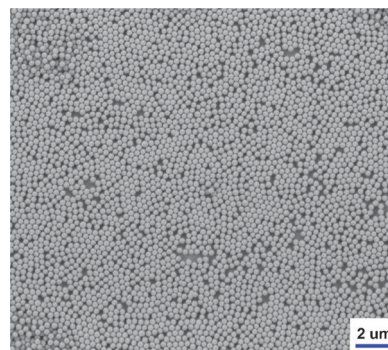


Fig. 3 FE-SEM image of SiO<sub>2</sub> particles on a SiO<sub>2</sub> plasma polymer modified QCM-crystal. Surface coverage was approximated with 1.1 monolayers resulting in a surface increase factor of 5.3 as discussed in the following section. The average particle diameter was found to be 250 nm.

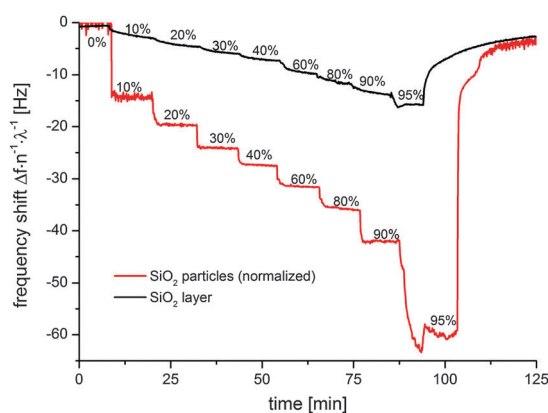


Fig. 4 QCM-D measurements of a smooth SiO<sub>2</sub> plasma polymer coated crystal (black) and the particle modified sample (red). Frequency shifts were divided by the order  $n$  of overtone observed and the surface increase factor  $\lambda$ . The surface increase factor for the correction was found to be 5.3 based on the SEM and BET data.

with SiO<sub>2</sub> spheres. The QCM-D data presented in Fig. 4 show high shifts towards smaller frequencies as a result of the mass change induced by the adsorbed water. However due to the coverage with nanoparticles the effective surface area also increases.

In order to compare the water uptake of the particle modified surface with the smooth SiO<sub>2</sub> plasma polymer the increase in effective surface area has to be considered. Assuming a perfectly smooth surface that is covered with a monolayer of hcp spheres, the effective surface increases. This factor can be calculated by basic geometric considerations. In the case of hcp a fundamental translation lattice can be defined (Fig. S5, ESI†) containing one particle.

Correlating the surface area of the particle with the projection area of the lattice results in a factor of  $2\pi/3^{-0.5} \approx 3.6$ . However in the case of the real sample and assuming that the particles are in point contact to the surface the substrate area itself cannot be neglected. Therefore, when comparing the particle modified substrate to the substrate without particles 1 has to be added to the surface increase factor accounting for the substrate area itself. In this simple model the substrate surface is approximated by a perfectly smooth plate. This approximation is supported





by the AFM data (Fig. S1A, ESI†) indicating that the real surface area is almost identical to the projection area. Moreover, the actual surface area of one particle could differ from the surface area of a perfect sphere due to a certain degree of surface roughness. BET measurements revealed the specific surface area to be  $12.68 \text{ m}^2 \text{ g}^{-1}$ . Taking the specific weight of  $\text{SiO}_2$  for Stöber particles<sup>21,22</sup> of  $2.04 \text{ g cm}^{-3}$  into account, the surface area of one specific particle with a diameter of 250 nm was calculated to be about  $0.21 \mu\text{m}^2$ . This value is in good agreement with the surface area of a perfectly smooth sphere of identical diameter which is approximately  $0.20 \mu\text{m}^2$ . Therefore, it is very likely that the used particles featured almost no roughness and the small deviation in particle surface area originates from the small and inevitable size distribution. Additionally in most cases, the prepared samples did not feature exactly one monolayer of particles. Taking all this into consideration the surface increase factor  $\lambda$  is given by:

$$\lambda = 1 + \frac{2\pi}{\sqrt{3}} \cdot \alpha \cdot \beta \quad (2)$$

where  $\alpha$  is the count of monolayers and  $\beta$  is the ratio between the surface area of a real particle based on the BET data and a perfect smooth sphere. Therefore, in the case of one single monolayer of ideal smooth spheres,  $\lambda$  is found to be 4.6. In order to correct the acquired QCM-D data for the increase of surface area all shifts are divided by  $\lambda$ . Prior to the QCM-D experiments, the actual surface coverage was determined by FE-SEM. In the case of the presented data, the surface coverage was approximated with 1.1 monolayers. Together with the BET data the resulting surface increase factor was found to be  $\approx 5.3$  for the presented dataset.

When comparing the corrected frequency shifts of the particle film coated substrate to the smooth  $\text{SiO}_2$  surface, it is obvious that the water uptake is significantly higher for the particle layer. This indicates that additional water has been adsorbed which is attributed to the formation of capillaries in the interparticle and particle-substrate contact areas.

The adsorption isotherm could be derived from the QCM-D data. For improved statistical reliability, the frequency shift values on each step were averaged and the mean shift was subsequently plotted *versus* the relative humidity as depicted in Fig. 5.

The adsorption isotherm on the  $\text{SiO}_2$  particle modified sample can roughly be divided into three segments. In the regime between 0 and 20% relative humidity, the transient is very steep and almost half of the total water layer has been adsorbed. This indicates that water adsorption is highly favorable for the hydrophilic surface. In the second segment ranging from 20% to 80% relative humidity the slope of the isotherm is rather low indicating that the surface is almost saturated. In the last section the high increase in slope indicates ongoing multilayer formation as well as capillary condensation in the particle layer. In contrast to the particle modified sample the smooth  $\text{SiO}_2$  plasma polymer layer exhibits a very linear increase in water uptake throughout the whole relative humidity range.

The corresponding dissipation data of the particle modified sample presented in Fig. 6 show an increase of dissipation until

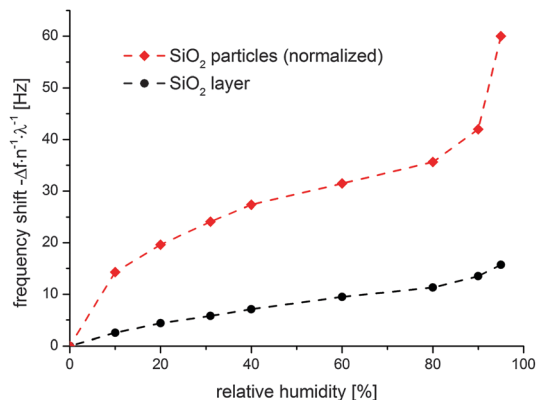


Fig. 5 Adsorption isotherm of water on the  $\text{SiO}_2$  plasma polymer (black) and  $\text{SiO}_2$  particle covered sample (red). Although the isotherm has been derived from the area corrected QCM-D data the total amount of water uptake is significantly higher than on the reference sample. This indicates that additional water is absorbed forming capillaries in the contact regions.

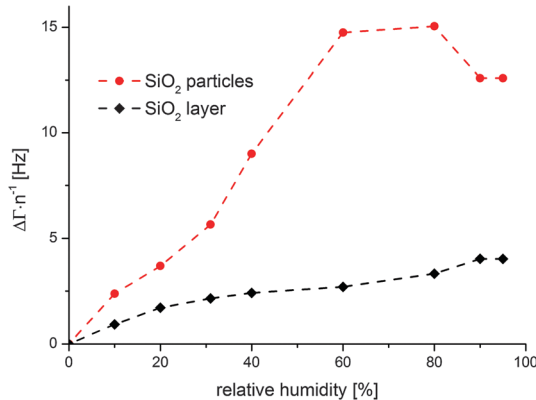


Fig. 6 Evolution of dissipation quantified by  $\Delta \Gamma$  during the experiment. In contrast to the dissipation curve on the smooth plasma polymer, the particle modified sample exhibits a maximum around 60% to 80% relative humidity. This behavior, originating from the change of contact mechanics due to capillary formation, has already been described by Dybwad<sup>10</sup> and Johannsmann.<sup>9</sup>

a maximum has been reached at about 60% to 80% relative humidity. A similar behavior has previously been described by Dybwad<sup>10</sup> and Johannsmann.<sup>9</sup> They found that the contact force between the particles and the resonator increased due to the formation of capillaries. Therefore the system changed from elastic (weak contact forces) to inertial loading (strong contact forces) resulting in the local maximum in the dissipation. We assume that a similar mechanism is responsible for the dissipation results in our case. However, during our experiment, the transitional capillary state is approached in the opposite direction.

In the experiment of Johannsmann *et al.*,<sup>9</sup> the fully wetted sample was slowly allowed to dry. During this process, the initially continuous water film slowly evaporated inducing the formation of capillaries. As a result, the contact force increased inducing a peak of the dissipation signal during the transition.

At variance, in the experiment presented within this work, the relative humidity is slowly increased. As a result, the capillaries



tend to grow according to the Kelvin equation. The growth of the capillaries results in two effects. On the one hand, the Laplace pressure decreases due to the larger capillary radius and on the other hand, the wetted area grows resulting in the increase of contact force. In the case of large particles, typically both effects cancel each other, resulting in a constant capillary force over a wide range of relative humidity values.<sup>23</sup> However, recent experiments performed by Asay *et al.*<sup>24</sup> indicated that this assumption does not hold true for nano-sized objects. They found that in the case of different alcohols, the capillary force is strongest in the low partial pressure region and decreases for higher partial pressures.

It is assumed that the same process occurs during the experiment performed within this work. In the initial state the spheres are strongly attached due to the high contact force based on the very small capillary radii. The subsequent increase of relative humidity leads to a decrease in contact force, until the system changes from inertial to elastic between 60% and 80% relative humidity. This transition causes the dissipation peak.

Moreover, the increased water uptake at high relative humidity (*e.g.* >80%) can be attributed to ongoing capillary growth and the beginning of a closed water film formation due to the merging of previously individual capillaries. In comparison to the particle modified sample, the smooth SiO<sub>2</sub> sample exhibits a much lower rather linear increase in dissipation with no maximum indicating the absence of a significant change in mechanical properties of the film.

### In situ FT-IR spectroscopy of water adsorption

FT-IR spectra were acquired simultaneously to the QCM-D experiment. All spectra were referenced to the spectra measured on the ODT sample at the same relative humidity. It was found that the OH-peak in the region of 3300 cm<sup>-1</sup> rises with increasing relative humidity indicating the adsorption of water on the particle surfaces. Moreover, in contrast to the measurement on the smooth SiO<sub>2</sub> layer, the intensity of the peak is dramatically higher which is in good agreement with the QCM-D data.

The FT-IR-data measured at 0% r.h. features a characteristic shoulder at ~3700 cm<sup>-1</sup> and a peak at around 3400 cm<sup>-1</sup> (Fig. 7). While the latter is mainly due to a single monolayer of water molecules adsorbed at the silanol groups of the silica surface,<sup>25</sup> the former indicates the presence of so called “free” or “dangling” OH groups of the surface silanols and/or of the adsorbed water monolayer,<sup>26,27</sup> respectively. The shoulder at ~3700 cm<sup>-1</sup> immediately decreases to zero when air of any relative humidity is being introduced to the measuring cell. The occurrence of the so called “ice-like” peak at around 3200 cm<sup>-1</sup> at higher relative humidity refers to the adsorption of multiple layers of water at the surface.

For a more detailed discussion, the measured spectra were deconvoluted as demonstrated in Fig. 8 for the measurement at 60% relative humidity. Previous publications<sup>13,27–30</sup> showed that the OH peak consists of multiple sub-peaks corresponding to vibrations of “liquid” (~3400 cm<sup>-1</sup>) and “ice-like” (3230 cm<sup>-1</sup> & 3117 cm<sup>-1</sup>) water as well as “free OH” (~3700 cm<sup>-1</sup>), respectively. Therefore, our fit consists of multiple components corresponding

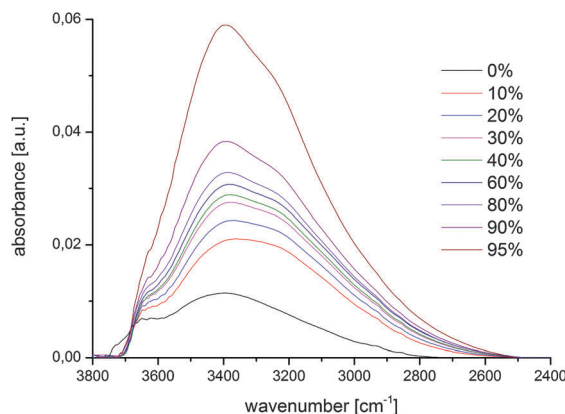


Fig. 7 FT-IR data of the SiO<sub>2</sub>-particle coated QCM-crystal. Presented spectra were measured simultaneously to the QCM-D data (Fig. 5 and 6). All spectra are referenced to the ODT SAM covered QCM-crystal measured under identical conditions (temperature, relative humidity, gas flow rate).

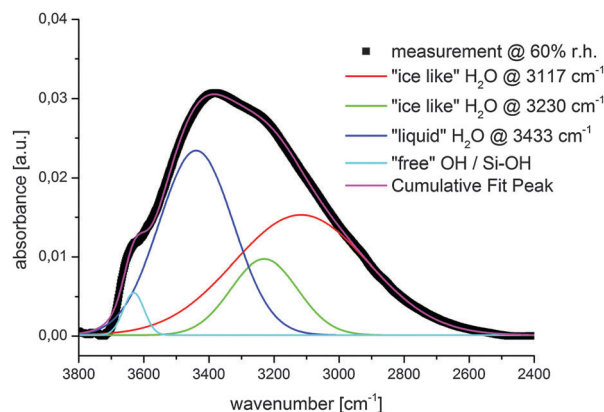


Fig. 8 Presentation of peak deconvolution of the OH peak in the region between 2400 cm<sup>-1</sup> and 3800 cm<sup>-1</sup> based on the dataset measured at 60% relative humidity. The peak has been fitted with four components in total, corresponding to “ice-like” H<sub>2</sub>O (3117 cm<sup>-1</sup> & 3230 cm<sup>-1</sup>), “liquid” H<sub>2</sub>O (~3400 cm<sup>-1</sup>), and “free” OH/Si-OH (~3600 cm<sup>-1</sup>).

to “ice-like” water (3117 cm<sup>-1</sup> and 3230 cm<sup>-1</sup>) as well as bulk liquid water (~3400 cm<sup>-1</sup>) and a rather general peak at around ~3650 cm<sup>-1</sup> that corresponds to dangling OH bonds of water molecules and/or silanol groups at low relative humidity. The presence of the “ice-like” peaks is due to the fact that at higher relative humidity multiple monolayers of water are adsorbed at the surface that are oriented similar to the water/air interface.<sup>27</sup> The corresponding peaks have been attributed to the hydrogen bonds between the first and second monolayer of water,<sup>28</sup> which is why the “ice-like” peaks are appearing at higher relative humidity only. However, as we have shown previously,<sup>29</sup> the peaks at 3400 cm<sup>-1</sup> and 3230 cm<sup>-1</sup> correspond to the symmetric and asymmetric stretching modes ( $\nu_1$  and  $\nu_2$ ) of liquid water molecules whose hydrogen-bond strengths are asymmetric.<sup>31,32</sup> As a consequence, the latter “ice-like” peak must be attributed to a liquid water configuration, in spite of the name. In contrast, the  $\nu_1$  and  $\nu_2$  coalesce into one peak at



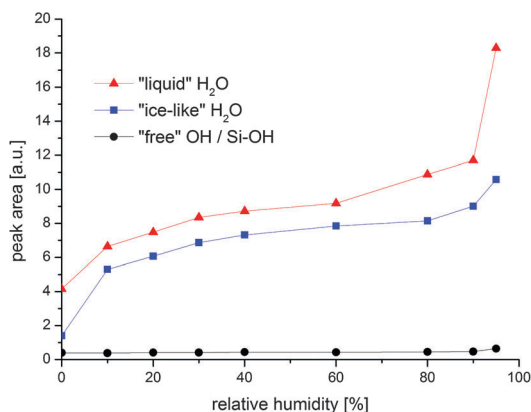


Fig. 9 Evolution of the peak area as a function of relative humidity. It can be seen that the peak of the "free" OH shows almost no change over the whole humidity range. The peak area corresponding to the "ice-like" H<sub>2</sub>O shows a very steep shape for low humidity, while for higher humidity the "liquid-like" signal shows a high increase in the peak area.

3117 cm<sup>-1</sup> whenever the hydrogen-bond strength becomes symmetric, *i.e.* "ice-like". The aforementioned peak at 3650 cm<sup>-1</sup>, which refers to free OH groups at low relative humidity, is consistent with the fleetingly broken hydrogen-bonds due to finite temperature within the bulk water portion at high relative humidity.<sup>26,32</sup> This is further supported by the fact that the associated peak area stays almost constant over the whole range of relative humidity (Fig. 9). This indicates that this contribution is either originating on the one hand from dangling OH bonds of water molecules and/or silanol groups at low relative humidity or, on the other hand, from dynamically broken OH bonds of bulk water molecules at high relative humidity. With respect to the former, the presence of surface Si-OH groups is in good agreement with the XPS data, which also indicates the presence of OH species based on the O 1s peak (Fig. S4, ESI†).

The detailed analysis of the OH peak region revealed the presence of a single monolayer of liquid water adsorbing to the particle surface and otherwise dangling OH groups of the water molecules and/or silanol groups under dry conditions. The steep increase in the peak area of the components corresponding to "ice-like" water indicates the presence of multiple monolayers of water as well as different absorption affinities at different sites.<sup>25</sup> At even higher humidity (>60%), the system more and more resembles bulk water as indicated by the strong increase in integrated area of the "liquid-like" peak. This is in good agreement with the corresponding dissipation data, which exhibit a local maximum between 60% and 80% relative humidity that can be attributed to the predominant growth of capillaries resulting in a decreased contact force (see previous section). The correlation of the dissipation data with the observed water structure implies that the particle substrate contact mechanics (indicated by the QCM-D) drastically changed at the same time when adsorption of "liquid-like water" starts to dominate. This might indicate that the lowering of the contact force during the inertial/elastic transition not only originates from the reduced Laplace pressure, but also from a change in the water adsorbate structure. In addition, both the

isotherm derived from the QCM-D data as well as the isotherm derived from the FT-IR data feature a similar trend. At low relative humidity both feature a very steep increase in water content followed by a low increase regime between 20% and 80% relative humidity. Moreover, both feature a steep increase at high relative humidity however the FT-IR data additionally indicate that the adsorbed water is predominantly of "liquid-like" nature which is in good agreement with the proposed capillary growth due to ongoing condensation.

## Conclusions

A new *in situ* analytical experimental setup combining FT-IR reflection absorption spectroscopy and QCM-D could be established for the investigation of water adsorption and capillary bridge formation in nano- and microparticle layers. The comparison of the water adsorption isotherms for SiO<sub>2</sub> nanoparticle layers with a smooth SiO<sub>2</sub>-like thin film allowed for the analysis of particle induced water layer formation in the contact regions.

It was shown that at low relative humidity only a single monolayer of water is adsorbed at the surface that gives rise to free OH bonds of the water molecules and/or the surface silanol groups. In contrast, at high humidity, the first two monolayers of water are oriented similar to the water/air interface, which entails the occurrence of the "ice-like" peaks in the FT-IR spectrum. Moreover, the comparison of the FT-IR and QCM-D data indicated a clear transition from an adsorbed layer to capillary bridges.

This finding was supported by the corresponding dissipation data exhibiting a local maximum between 60% and 80% relative humidity indicating a decrease in contact force due to the growth of capillaries in agreement to former studies reported by Johannsmann *et al.*<sup>9</sup>

The presented results illustrate that the combination of *in situ* FT-IR and QCM-D data enables the qualitative and quantitative analysis of water adsorption and capillary bridge formation in particle layers.

## Acknowledgements

We gratefully acknowledge the Deutsche Forschungsgemeinschaft for financial support within the "Schwerpunktprogramm Partikel im Kontakt" DFG-SPP 1486. We also thank Mr Dominik Klaus from the group of Prof. Tiemann (University of Paderborn) for performing the BET measurements. CZ and TDK acknowledge financial support from the Graduate School of Excellence MAINZ and the IDEE project of the Carl Zeiss Foundation.

## Notes and references

- 1 H. Kong and J. Jang, *Langmuir*, 2008, **24**, 2051–2056.
- 2 I. Sondi and B. Salopek-Sondi, *J. Colloid Interface Sci.*, 2004, **275**, 177–182.
- 3 M.-C. Daniel and D. Astruc, *Chem. Rev.*, 2004, **104**, 293–346.
- 4 D. Astruc, F. Lu and J. R. Aranzaes, *Angew. Chem., Int. Ed.*, 2005, **44**, 7852–7872.



- 5 J. N. Israelachvili, *Intermolecular and surface forces: revised third edition*, Academic press, 2011.
- 6 M. Farshchi-Tabrizi, M. Kappl, Y. Cheng, J. Gutmann and H.-J. Butt, *Langmuir*, 2006, **22**, 2171–2184.
- 7 H.-J. Butt, M. Makowski, M. Kappl and A. Ptak, *KONA*, 2011, **29**, 2011.
- 8 J. N. D'Amour, J. J. R. Stalgren, K. K. Kanazawa, C. W. Frank, M. Rodahl and D. Johannsmann, *Phys. Rev. Lett.*, 2006, **96**, 05831.
- 9 B. Y. Du, A. M. König and D. Johannsmann, *New J. Phys.*, 2008, **10**, 053014.
- 10 G. Dybwad, *J. Appl. Phys.*, 1985, **58**, 2789.
- 11 A. Pomorska, K. Yliniemi, B. P. Wilson, D. Shchukin, D. Johannsmann and G. Grundmeier, *J. Colloid Interface Sci.*, 2011, **362**, 180–187.
- 12 A. Pomorska, D. Shchukin, R. Hammond, M. A. Cooper, G. Grundmeier and D. Johannsmann, *Anal. Chem.*, 2010, **82**, 2237–2242.
- 13 D. B. Asay and S. H. Kim, *J. Phys. Chem. B*, 2005, **109**, 16760–16763.
- 14 I. Giner, M. Maxisch, C. Kunze and G. Grundmeier, *Appl. Surf. Sci.*, 2013, **283**, 145–153.
- 15 R. Vlasak, I. Klueppel and G. Grundmeier, *Electrochim. Acta*, 2007, **52**, 8075–8080.
- 16 K. Wapner, M. Stratmann and G. Grundmeier, *Electrochim. Acta*, 2006, **51**, 3303–3315.
- 17 C. N. Liu, B. Ozkaya, S. Steves, P. Awakowicz and G. Grundmeier, *J. Phys. D: Appl. Phys.*, 2013, **46**, 084013.
- 18 N. A. Chumaevskii and M. N. Rodnikova, *J. Mol. Liq.*, 2003, **106**, 167–177.
- 19 Q. Du, E. Freysz and Y. R. Shen, *Science*, 1994, **264**, 826–828.
- 20 M. Creatore, F. Palumbo, R. d'Agostino and P. Fayet, *Surf. Coat. Technol.*, 2001, **142**, 163–168.
- 21 G. H. Bogush, M. A. Tracy and C. F. Zukoski Iv, *J. Non-Cryst. Solids*, 1988, **104**, 95–106.
- 22 M. Kobayashi, M. Skarba, P. Galletto, D. Cakara and M. Borkovec, *J. Colloid Interface Sci.*, 2005, **292**, 139–147.
- 23 H.-J. Butt and M. Kappl, *Surface and interfacial forces*, John Wiley & Sons, 2009.
- 24 D. Asay, M. De Boer and S. Kim, *J. Adhes. Sci. Technol.*, 2010, **24**, 2363–2382.
- 25 M. Sulpizi, M.-P. Gaigeot and M. Sprik, *J. Chem. Theory Comput.*, 2012, **8**, 1037–1047.
- 26 T. D. Kühne, M. Krack and M. Parrinello, *J. Chem. Theory Comput.*, 2009, **5**, 235–241.
- 27 T. D. Kühne, T. A. Pascal, E. Kaxiras and Y. Jung, *J. Phys. Chem. Lett.*, 2010, **2**, 105–113.
- 28 Y. Fan, X. Chen, L. Yang, P. S. Cremer and Y. Q. Gao, *J. Phys. Chem. B*, 2009, **113**, 11672–11679.
- 29 C. Zhang, R. Z. Khaliullin, D. Bovi, L. Guidoni and T. D. Kühne, *J. Phys. Chem. Lett.*, 2013, **4**, 3245–3250.
- 30 C. Ratcliffe and D. Irish, *J. Phys. Chem.*, 1982, **86**, 4897–4905.
- 31 T. D. Kühne and R. Z. Khaliullin, *Nat. Commun.*, 2013, **4**, 1450.
- 32 R. Z. Khaliullin and T. D. Kühne, *Phys. Chem. Chem. Phys.*, 2013, **15**, 15746–15766.

